


Investigating the origin of pH-sensitive magnetization transfer ratio asymmetry MRI contrast during the acute stroke: Correction of T_1 change reveals the dominant amide proton transfer MRI signal

Limin Wu¹ | Liang Jiang^{2,3} | Phillip Zhe Sun^{3,4,5} 

¹Neuroscience Center and Department of Pediatrics, Massachusetts General Hospital and Harvard Medical School, Charlestown, Massachusetts, USA

²Department of Otolaryngology, Head and Neck Surgery, Affiliated Hospital of Southwestern Medical University, Luzhou, Sichuan, China

³Yerkes Imaging Center, Yerkes National Primate Research Center, Emory University, Atlanta, Georgia, USA

⁴Department of Radiology and Imaging Sciences, Emory University School of Medicine, Atlanta, Georgia, USA

⁵Athinoula A. Martinos Center for Biomedical Imaging, Department of Radiology, Massachusetts General Hospital and Harvard Medical School, Charlestown, Massachusetts, USA

Correspondence

Phillip Zhe Sun, Department of Radiology and Imaging Sciences, Emory University School of Medicine, 954 Gatewood Road NE, Atlanta, GA 30329, USA.
Email: pzhesun@emory.edu

Funding information

National Institute of Neurological Disorders and Stroke, Grant/Award Number: R01NS083654

Purpose: Amide proton transfer (APT) MRI is promising to serve as a surrogate metabolic imaging biomarker of acute stroke. Although the magnetization transfer ratio asymmetry (MTR_{asym}) has been used commonly, the origin of pH-weighted MRI effect remains an area of investigation, including contributions from APT, semi-solid MT contrast asymmetry, and nuclear Overhauser enhancement effects. Our study aimed to determine the origin of pH-weighted MTR_{asym} contrast following acute stroke.

Methods: Multiparametric MRI, including T_1 , T_2 , diffusion and Z-spectrum, were performed in rats after middle cerebral artery occlusion. We analyzed the conventional Z-spectrum $\left(\frac{I(\Delta\omega)}{I_0}\right)$ and the apparent exchange spectrum $(R_{\text{ex}}(\Delta\omega))$, being the difference between the relaxation-scaled inverse Z-spectrum and the intrinsic spin-lock relaxation rate $\left(R_1 \cdot \cos^2\theta \cdot \frac{I_0}{I(\Delta\omega)} - R_{1\rho}(\Delta\omega)\right)$. The ischemia-induced change was calculated as the spectral difference between the diffusion lesion and the contralateral normal area.

Results: The conventional Z-spectrum signal change at -3.5 ppm dominates that at $+3.5$ ppm ($-1.16 \pm 0.39\%$ vs. $0.76 \pm 0.26\%$, $P < .01$) following acute stroke. In comparison, the magnitude of ΔR_{ex} change at 3.5 ppm becomes significantly larger than that at -3.5 ppm ($-2.80 \pm 0.40\%$ vs. $-0.94 \pm 0.80\%$, $P < .001$), with their SNR being 7.0 and 1.2, respectively. We extended the magnetization transfer and relaxation normalized APT concept to the apparent exchange-dependent relaxation image, documenting an enhanced pH contrast between the ischemic lesion and the intact tissue, over that of MTR_{asym} .

Limin Wu and Liang Jiang contributed equally to this work.

Conclusion: Our study shows that after the relaxation-effect correction, the APT effect is the dominant contributing factor to pH-weighted MTR_{asym} following acute stroke.

KEYWORDS

acute stroke, amide proton transfer, apparent exchange-dependent relaxation, chemical exchange saturation transfer, magnetization transfer and relaxation normalized APT, pH

1 | INTRODUCTION

Brain-tissue pH drops following sudden hypoperfusion, which disrupts cerebral oxygen and glucose metabolism, making pH a surrogate metabolic biomarker of acute ischemic tissue.^{1,2} Amide proton transfer (APT) MRI is a form of CEST imaging, which provides noninvasive intracellular pH-weighted mapping.³⁻¹⁰ The commonly used pH-weighted magnetization transfer (MT) ratio asymmetry (MTR_{asym}) analysis takes the signal difference between -3.5 and 3.5 ppm to correct for the direct RF saturation effect. It has been shown that pH-weighted MRI refines heterogeneous perfusion/diffusion lesion mismatch into perfusion/pH lesion mismatch and pH/diffusion lesion mismatch, postulated to represent the benign oligemia and metabolic penumbra, respectively.^{11,12} The APT-weighted MRI has been translated to study acute stroke patients with preliminary yet promising results.¹³⁻¹⁵ Recently, it has been demonstrated that MT and relaxation-normalized APT (MRAPT) analysis minimizes the concomitant non-pH-dependent factors, resulting in enhanced correlation with tissue pH over that of MTR_{asym} .¹⁶⁻¹⁸ Nevertheless, MTR_{asym} and its variants provide a mixed contrast, and tremendous efforts have been devoted to elucidating the origin of pH-weighted MRI, which may further improve pH measurement.¹⁹⁻²³

The assumption that the pH-dependent APT effect dominates the pH-weighted MTR_{asym} measurement was, in large part, built on the evidence that in cardiac-arrest global ischemia rodent models, the Z-spectral signal had little change at -3.5 ppm, whereas it increased at $+3.5$ ppm.⁴ However, the source of pH-weighted MTR_{asym} contrast has often been debated. For example, Watanabe et al concluded that the dipolar coupling between aliphatic and water protons rather than proton exchange is the dominant factor in Z-spectra and MTR_{asym} in the brain.²⁴ Li et al and Heo et al reported significant nuclear Overhauser enhancement (NOE) and APT changes in acute stroke.^{21,25} Wu et al showed that NOE and MT-contrast changes counteracted each other, leaving the net MTR_{asym} change dominated by the APT effect in an acute stroke rodent model.²² In a global ischemia model, Zhou et al showed that the negative MT-contrast asymmetry change is about the same magnitude of the APT effect.²³ As such, the origin of pH-weighted MTR_{asym} signal following acute stroke is complex and unsettled, which casts doubt on the accuracy of pH

mapping. Particularly, it has been documented that the experimentally measurable CEST-MRI effect strongly depends on T_1 ,²⁶⁻³¹ yet the impact of T_1 on acute stroke pH imaging has not been thoroughly investigated. Moreover, early T_1 change has been reported following the experimental acute stroke.³²⁻³⁵ Kaur et al also showed T_1 change in transient stroke models.³⁶ These results are consistent with the work of Young et al, which demonstrated a high correlation between net ion shift and edema in acute stroke.³⁷ We also showed that T_1 -normalized MTR_{asym} is of higher pH correlation over MTR_{asym} , enabling improved pH imaging.^{8,9} Herein, our study aimed to take into account the T_1 contribution, and determine the source of in vivo MTR_{asym} signal change in an animal model of acute stroke. Although the conventional Z-spectrum suggested that the magnitude change in NOE signal dominates that of the APT, our data also showed significant tissue-relaxation change during the acute stroke phase. To account for such relaxation changes, we calculated the difference between the relaxation-scaled inverse Z-spectrum and the intrinsic spinlock relaxation rate ($R_{\text{ex}}(\Delta\omega) = R_1 \cdot \cos^2\theta \cdot \frac{I_0}{I(\Delta\omega)} - R_{1\rho}(\Delta\omega)$), which showed that the observed NOE effect in the conventional Z-spectrum was primarily attributed to a symmetric signal intensity change around the water frequency. After accounting for the relaxation change, the APT signal is restored and becomes the dominating source of pH-weighted MRI contrast. Capitalizing on this finding, we also generalized the MRAPT concept to the apparent exchange-dependent relaxation (AREX) image for pH-specific mapping.^{16,17}

2 | THEORY

The CEST-MRI effect is often quantified by normalizing the saturated scans ($I(\Delta\omega)$) with the unsaturated control scan (I_0). The steady-state CEST-MRI signal is given as^{38,39}

$$\frac{I(\Delta\omega)}{I_0} = \frac{R_1 \cdot \cos^2\theta}{R_{1\rho}^{\text{ex}}(\Delta\omega)}, \quad (1)$$

where $R_{1\rho}^{\text{ex}}(\Delta\omega) = R_1 \cos^2\theta + R_2 \sin^2\theta + R_{\text{ex}}(\Delta\omega)$; $\theta = \text{atan}\left(\frac{\gamma B_1}{\Delta\omega}\right)$, in which γ is the gyromagnetic ratio; R_1 and R_2 are the bulk water longitudinal and transverse relaxation rates, respectively, with B_1 and $\Delta\omega$ being the amplitude and offset of the RF irradiation;

and $R_{\text{ex}}(\Delta\omega)$ describes the multipool CEST and semisolid MT effects. We have $R_{\text{ex}}(\Delta\omega) = \sum_{i=1}^N f_{si} \cdot k_{swi} \cdot \alpha_i$, where f_{si} and k_{swi} are the i th pool labile proton ratio and exchange rate, respectively, and α_i is the corresponding labeling coefficient. Equation 1 shows that the conventional Z-spectrum $\left(\frac{I(\Delta\omega)}{I_0}\right)$ depends on both the intrinsic longitudinal relaxation rate and the spinlock relaxation rate ($R_{1p} = R_1 \cos^2\theta + R_2 \sin^2\theta$), the correction of which may improve the specificity of CEST-MRI measurement to the labile proton ratio and exchange rate.

It has been shown that the inverse normalization $\left(\frac{I_0}{I(\Delta\omega)}\right)$ simplifies the quantification of multipool CEST effects from that using the unsaturated scan–denominated conventional Z-spectrum.³⁰ We have

$$\frac{I_0}{I(\Delta\omega)} = \frac{R_{1p}^{\text{ex}}(\Delta\omega)}{R_1 \cdot \cos^2\theta}. \quad (2)$$

The R_1 -scaled inversely normalized CEST signal reduces the nonlinear coupling to a linear summation of multipool CEST and semisolid MT effects as follows:

$$R_{1p}^{\text{ex}}(\Delta\omega) = R_1 \cdot \cos^2\theta \cdot \frac{I_0}{I(\Delta\omega)}. \quad (3)$$

The CEST effect change following acute ischemia can be determined by subtracting the intrinsic spin lock relaxation rate from the R_1 -scaled inverse Z-spectral analysis. Specifically, we obtain

$$R_{\text{ex}}(\Delta\omega) = R_{1p}^{\text{ex}}(\Delta\omega) - R_{1p}(\Delta\omega) = R_1 \cdot \cos^2\theta \cdot \frac{I_0}{I(\Delta\omega)} - (R_1 \cos^2\theta + R_2 \sin^2\theta). \quad (4)$$

3 | METHODS

3.1 | Animals

In vivo studies have been approved by the Institutional Animal Care and Use Committee, Massachusetts General Hospital. We performed multiparametric MRI in 12 adult male Wistar rats following acute stroke. Anesthesia was induced in rats with 5% isoflurane and air mixture for 5 minutes and then maintained under 1.5%-2% isoflurane for the duration of the surgery and imaging. We monitored rat heart rate and blood oxygen saturation throughout the experiment (Nonin Pulse Oximeter 8600, Plymouth, MN) with their core temperature maintained by a circulating warm water jacket surrounding the torso. We used a classical middle cerebral artery occlusion stroke model by gently inserting a 4-0 silicone-coated nylon suture through the internal carotid artery to block the

origin of the middle cerebral artery. Rats were imaged between 1 and 2 hours after the middle cerebral artery occlusion operation. One rat displayed a tiny hypothalamic lesion without striatal and cortical lesions, and the animal was excluded from the data analysis.

3.2 | Magnetic resonance imaging

All MRI scans were performed using a 4.7T small-bore Bruker MRI system (Bruker Biospec, Ettlingen, Germany). We used single-shot EPI with a FOV of $20 \times 20 \text{ mm}^2$ (matrix = 48×48 , slice thickness/slice gap = 1.8/0.2 mm, 5 slices). We acquired multiparametric MRI scans, including perfusion, diffusion, water-saturation shift reference, Z-spectrum, APT-weighted, and T_1 -weighted and T_2 -weighted scans. Specifically, perfusion imaging was acquired using amplitude-modulated arterial spin labeling MRI (TR/TE = 5000/20 ms, arterial spin labeling tagging time = 3000 ms, 32 averages, scan time = 5 minutes 36 seconds).⁴⁰ Diffusion imaging was obtained with a single-shot isotropic diffusion-weighted MRI (two b-values of 250 and 1000 s/mm^2 , TR/TE = 3250/42 ms, 16 averages, scan time = 1 minute 44 seconds).⁴¹ A water-saturation shift-reference scan was obtained to map the B_0 field inhomogeneity ($B_1 = 0.5 \mu\text{T}$, relaxation delay = 3000 ms, saturation time = 250 ms) from -0.5 to 0.5 ppm with intervals of 0.05 ppm.⁴² For Z-spectrum and APT-weighted MRI, we used a CEST-MRI sequence with an unevenly segmented RF irradiation, which includes a long (primary) saturation pulse that drives to the CEST steady-state and short (secondary) saturation pulses between image readout and average loops that maintain the CEST steady state for fast and sensitive imaging.⁴³ We collected Z-spectrum from -6 to 6 ppm with intervals of 0.25 ppm ($B_1 = 0.75 \mu\text{T}$, relaxation delay = 3500 ms, primary saturation time = 3000 ms, secondary saturation time = 500 ms, four averages, and scan time = 13 minutes 20 seconds). In addition, we performed three-point APT-weighted scans, with eight averages of the unsaturated control scan and 32 averages of saturated scans at ± 3.5 ppm (scan time = 4 minutes). Moreover, T_1 -weighted inversion-recovery images were acquired with inversion time (TI) ranging from 250 ms to 3000 ms (relaxation delay/TE = 6500/20 ms, four averages, and scan time = 3 minutes 38 seconds), and T_2 -weighted MRI was obtained with two separate spin-echo EPI scans (TR/TE1/TE2 = 3250/30/100 ms, 16 averages, and scan time = 1 minute 40 seconds).

3.3 | Data analysis

Images were processed in *MATLAB* R2019a (MathWorks, Natick, MA). Parametric T_1 , T_2 , and ADC maps were obtained using least-squares mono-exponential

fitting of the signal intensities as functions of the TI ($I = I_0 \left| 1 - (2 - \eta \cdot e^{-T_d/T_1}) \cdot e^{-TI/T_1} \right|$, where η is the inversion efficiency and T_d is the relaxation delay, TE ($I = I_0 e^{-TE/T_2}$), and diffusion b-value ($I = I_0 e^{-b \cdot ADC}$), respectively. The cerebral blood flow (CBF) was calculated using $CBF = \frac{\lambda}{T_1} \cdot \frac{I_{ref} - I_{tag}}{2\alpha \cdot I_{ref}}$, where λ is the brain/blood partition coefficient, I_{tag} and I_{ref} are arterial spin labeling tagging and reference images, respectively, and α is the degree of blood spin inversion.⁴⁰ The B_0 field inhomogeneity was determined from the water-saturation shift-reference scan and applied to correct Z-spectrum.⁴² The Z spectrum was analyzed using both the unsaturated scan denominated normalization ($Z = \frac{I(\Delta\omega)}{I_0}$) and the inverse Z-spectrum analysis approach ($Z_{inv} = \frac{I_0}{I(\Delta\omega)}$). The R_{ex} spectrum was calculated using Equation 4. In addition, APT-weighted images were processed using $MTR_{asym} \left(\frac{I(-3.5 \text{ ppm}) - I(+3.5 \text{ ppm})}{I_0} \right)$, T_1 -normalized $MTR_{asym} \left(R_1 \cdot \frac{I(-3.5 \text{ ppm}) - I(+3.5 \text{ ppm})}{I_0} \right)$, and AREX $\left(R_1 \cos^2 \theta \cdot \left(\frac{I_0}{I(+3.5 \text{ ppm})} - \frac{I_0}{I(-3.5 \text{ ppm})} \right) \right)$. The ischemic diffusion lesion was automatically segmented from the ADC map using a K-means clustering algorithm of two clusters, with the label for the ischemic lesion automatically identified as the cluster of a reduced ADC.⁴⁴ The ipsilateral ischemic lesion was mirrored to the contralateral brain along the midline.²²

The pH-specific MRAPT analysis ($\Delta MRAPTR$) is calculated as the difference between R_1 -scaled MTR_{asym} and an estimated baseline image that is not pH-dependent.¹⁵⁻¹⁷ Briefly, we have

$$\Delta MRAPTR \approx (R_1 \cdot MTR_{asym})_{ischemic} - F(R_1, MMTR) \approx (f_s \cdot k_{sw})_{ischemic} - (f_s \cdot k_{sw})_{norm} \quad (5)$$

where $F(R_1, MMTR)$ is the non-pH-dependent baseline image estimated from R_1 and mean MTR at ± 3.5 ppm (MMTR) maps. Note that it has been shown that MMTR has less change than $MTR(+3.5 \text{ ppm})$ and $MTR(-3.5 \text{ ppm})$ following acute stroke.¹⁶ Because it is generally believed that pH dominates

the APT-weighted effect during the acute stroke; we have $(f_s \cdot k_{sw})_{ischemic} - (f_s \cdot k_{sw})_{norm} \approx f_s \cdot \Delta k_{sw}$, with Δk_{sw} being an acidosis-induced drop in the exchange rate. Our study further generalized the concept of MRAPT analysis to $R_{ex}(+3.5 \text{ ppm})$, $R_{ex}(-3.5 \text{ ppm})$, and AREX images. Briefly, we evaluated the pixel-wise regression between R_1 , MMTR, and the image of interest ($R_{ex}(+3.5 \text{ ppm})$, $R_{ex}(-3.5 \text{ ppm})$, and AREX) in the contralateral healthy brain. The derived regression coefficients were then applied to correct the concomitant non-pH-dependent image baseline shift across the brain, following Equation 5.^{16,17}

We evaluated region of interest (ROI)-based multiparametric MRI changes between the ipsilateral diffusion lesion and contralateral normal area. The contrast-to-noise ratio (CNR) from each animal was calculated as the ratio of the ROI intensity difference over the mean SD $\left(\sqrt{(\sigma_{norm}^2 + \sigma_{ischemic}^2) / 2} \right)$, calculated from the ROI of the contralateral normal area and ischemic diffusion lesion. The group mean CNR and its SD were summarized from the CNR of each rat. Also, Cohen's d was calculated as the difference of the mean value over the mean SD from all acute stroke rats. Two sample *t*-tests of equal variance were performed to evaluate the ischemia-induced MRI changes, and *p*-values less than .05 were regarded as statistically significant.

4 | RESULTS

Figure 1 shows T_1 (Figure 1A), T_2 (Figure 1B), ADC (Figure 1C), and MTR_{asym} (Figure 1D) maps of a representative acute stroke rat between 1 and 2 hours after middle cerebral artery occlusion. There was a small yet significant T_1 increase (from 1.54 ± 0.03 to 1.65 ± 0.04 s, $P < .01$) following acute ischemia. There was also a minimal yet significant T_2 decrease (from 53.67 ± 0.73 to 52.85 ± 0.56 ms, $P < .01$; Figure 1B). In addition, the ischemic lesion displayed a clear ADC drop from that of the healthy tissue (0.65 ± 0.02 vs. $0.83 \pm 0.03 \mu\text{m}^2/\text{ms}$, $P < .001$). The number of diffusion lesion pixels were 308 ± 73 pixels (mean \pm SD), ranging from

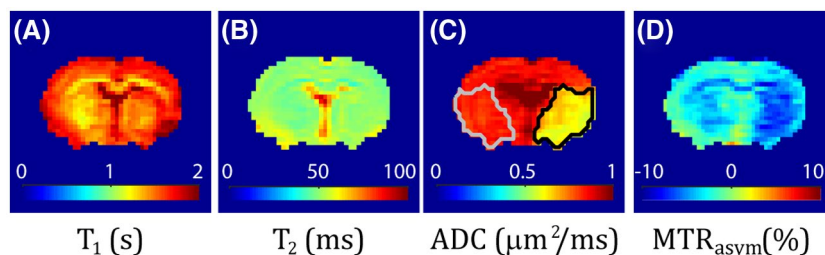


FIGURE 1 Multiparametric images of a representative acute stroke rat. A, The T_1 map. B, The T_2 map. C, The ADC map with the diffusion lesion and contralateral normal areas outlined in black and gray lines, respectively. D, The pH-weighted magnetization transfer ratio asymmetry (MTR_{asym}) map

214 to 462 pixels (median = 314 pixels). In addition, the pH-weighted MTR_{asym} image showed a signal drop in the ipsilateral lesion from that of the contralateral normal area ($-5.46 \pm 0.51\%$ vs. $-3.57 \pm 0.61\%$, $P < .001$). Table 1 summarizes values from the diffusion lesion and the contralateral normal area, and their differences from all stroke rats ($n = 11$). The multiparametric images from all acute stroke rats are shown in Supporting Information Figures S1-S10.

We first quantified the ischemia-induced signal change using conventional Z-spectrum. Figure 2A overlays Z-spectra from the contralateral normal area (red) and ischemic diffusion lesion (blue) of a representative acute stroke rat, the same one as in Figure 1. There appeared to be a subtle Z-spectral signal elevation at 3.5 ppm in the ischemic lesion, suggesting a slight reduction in the exchange rate, and hence, pH drop. However, the most prominent feature was a decrease in signal intensity over the aliphatic frequency range. Figure 2B shows the Z-spectral difference ($Z_{\text{ipsi}} - Z_{\text{contra}}$) between the contralateral normal and ipsilateral ischemic regions (black diamond markers). The normalized signal change at -3.5 ppm dominated that at $+3.5$ ppm ($-1.16 \pm 0.39\%$ vs. $0.76 \pm 0.26\%$, $P < .01$). Note that the increase in the signal change at $+3.5$ ppm means a reduced APT effect and acidosis. To better visualize the Z-spectral signal change, Figure 2C shows the MTR_{asym} spectra from the contralateral normal (red) and ipsilateral ischemic (blue) regions. Similar to Figure 2B, there was a small signal drop at 3.5 ppm in addition to a pronounced baseline shift from that of the contralateral normal tissue. Figure 2D shows the MTR_{asym} spectral difference between the ischemic and contralateral normal regions. A summary of Figure 2 from all acute stroke rats is shown in Supporting Information Figure S11.

We also analyzed R_1 -scaled inversely normalized Z-spectrum ($R_{1\rho}^{\text{ex}}(\Delta\omega) = R_1 \cdot \frac{I_0 \cos^2\theta}{I(\Delta\omega)}$) following acute stroke. Figure 3A shows that the R_1 -scaled inverse Z-spectrum from

the diffusion lesion decreased substantially from that of the contralateral normal area of a representative acute stroke rat, the same one as in Figure 2. Because R_1 -scaled inversely normalized Z-spectrum is truncated at 0 ppm, it is not straightforward to compare the linewidth with that of Figure 2A. The value of $R_{1\rho}^{\text{ex}}$ includes contributions from both CEST effects (R_{ex}) and intrinsic bulk tissue water ($R_{1\rho}$). The value of $R_{1\rho}$ was calculated from parametric T_1 and T_2 maps. Figure 3B shows that $R_{1\rho}(\pm 3.5 \text{ ppm})$ decreased from 0.69 ± 0.02 (contralateral normal area) to 0.65 ± 0.02 (ischemic diffusion lesion, $P < .001$). Figure 3C shows R_{ex} spectra ($R_{\text{ex}}(\Delta\omega) = R_{1\rho}^{\text{ex}}(\Delta\omega) - R_{1\rho}(\Delta\omega)$) from the diffusion lesion (blue) and the contralateral normal (red) area. The R_{ex} spectra overlapped reasonably well at the aliphatic chemical shifts, while the signal change at $+3.5$ ppm emerged as the dominant factor of change. Figure 3D shows the R_{ex} difference (ΔR_{ex}) between the normal and ischemic regions. A summary of Figure 3 from all acute stroke rats is shown in Supporting Information Figure S12. Across all animals, the signal change at $+3.5$ ppm dominates that at -3.5 ppm ($-2.804 \pm 0.396\%$ vs. $-0.944 \pm 0.799\%$, $P < .001$), with their SNRs being 7.0 and 1.2, respectively.

Figure 4 shows the multiparametric image characterization of pH-weighted MRI. Although the $MMTR(\pm 3.5 \text{ ppm})$ image showed little change after acute ischemia (Figure 4A), there was a noticeable $R_{1\rho}$ decrease (Figure 4B). The R_1 -scaled inversely normalized images showed a more pronounced signal change at $+3.5$ ppm (Figure 4D) than that of -3.5 ppm (Figure 4C). The R_{ex} images were obtained by subtracting the calculated $R_{1\rho}$ map from the R_1 inversely normalized CEST images. Figure 4F shows that $R_{\text{ex}}(+3.5 \text{ ppm})$ has a more noticeable signal drop in the ipsilateral ischemic area than that of $R_{\text{ex}}(-3.5 \text{ ppm})$ in Figure 4E. Nevertheless, R_{ex} images (Figure 4E,F) are susceptible to concomitant semisolid MT contrast (3.5 ppm) and MT contrast plus NOE

TABLE 1 Comparison of multiparametric MRI from the ipsilateral ischemic lesion and the contralateral normal area, and their difference

	Contralateral normal area	Ipsilateral ischemic area	Difference
T_1 (seconds)	1.54 ± 0.03	$1.65 \pm 0.04^*$	0.109 ± 0.021
T_2 (ms)	53.67 ± 0.73	$52.85 \pm 0.56^{**}$	-0.821 ± 0.481
CBF (mL/g•min)	1.00 ± 0.19	$0.53 \pm 0.10^{***}$	-0.465 ± 0.110
ADC ($\mu\text{m}^2/\text{ms}$)	0.83 ± 0.03	$0.65 \pm 0.02^{***}$	-0.185 ± 0.019
$I/I_0(-3.5 \text{ ppm})$	0.68 ± 0.01	$0.67 \pm 0.01^{***}$	$-1.155\% \pm 0.390\%$
$I/I_0(+3.5 \text{ ppm})$	0.72 ± 0.01	0.72 ± 0.01	$0.761 \pm 0.260\%$
$MMTR(\pm 3.5 \text{ ppm})$	0.30 ± 0.01	0.30 ± 0.01	$0.197\% \pm 0.236\%$
MTR_{asym}	$-3.57\% \pm 0.61\%$	$-5.46\% \pm 0.51\%^{***}$	$-1.891\%/s \pm 0.424\%$
$R_{1\rho}(\pm 3.5 \text{ ppm})$	0.69 ± 0.02 (1/s)	$0.65\% \pm 0.02\%$ (1/s) ***	$-4.417\%/s \pm 0.798\%/s$
$\Delta R_{\text{ex}}(-3.5 \text{ ppm})$	0.27 ± 0.01 (1/s)	0.26 ± 0.01 (1/s)	$-0.944\%/s \pm 0.799\%/s$
$\Delta R_{\text{ex}}(+3.5 \text{ ppm})$	0.22 ± 0.01 (1/s)	0.19 ± 0.01 (1/s) ***	$-2.804\%/s \pm 0.396\%/s$

Note: Two sample t -tests of equal variance were performed to evaluate the ischemia-specific changes.

* $P < .01$; ** $P < .05$; *** $P < .001$.

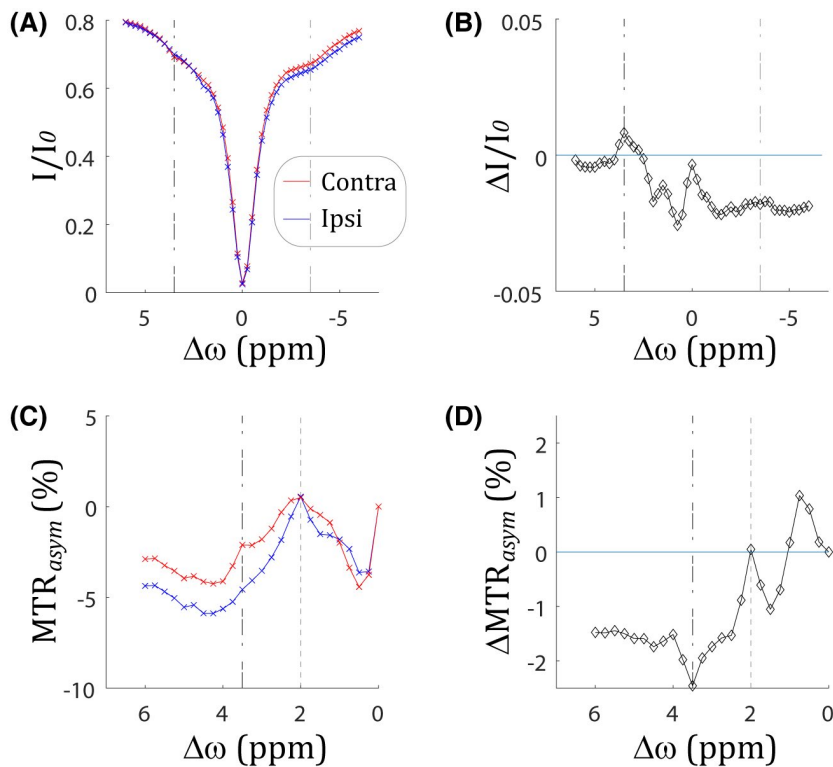


FIGURE 2 Characterization of ischemia-induced CEST Z-spectral signal change. A, The CEST Z-spectra obtained from the contralateral normal area (red) and ipsilateral ischemic region (blue). B, Z-spectral signal change between the contralateral normal area and the ipsilateral ischemic region. C, The MTR_{asym} spectra from the contralateral normal area (red) and ipsilateral ischemic region (blue). D, The MTR_{asym} spectral difference between the contralateral normal area and ipsilateral ischemic lesion

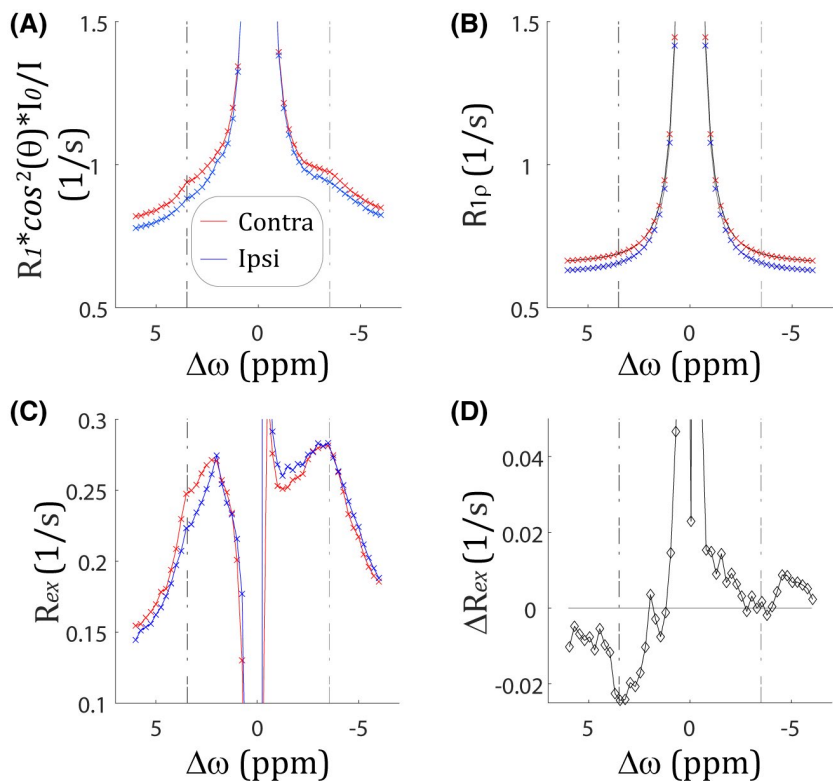


FIGURE 3 Characterization of ischemia-induced inverse CEST Z-spectral signal change. A, The R_1 -scaled inverse CEST Z-spectral changes between the contralateral normal area (red) and ipsilateral ischemic region (blue). B, Intrinsic $R_{1\rho}$ spectral changes between the contralateral normal area (red) and the ipsilateral ischemic region (blue). C, The R_{ex} spectral changes between the contralateral normal area (red) and the ipsilateral ischemic region (blue). D, The R_{ex} spectral difference between the contralateral normal area and ipsilateral ischemic lesion

effects (-3.5 ppm), respectively, resulting in nonuniformity across the intact brain. We generalized the concept of MRAPT analysis^{16,17} to minimize non-pH-dependent image heterogeneity in R_{ex} (± 3.5 ppm) images, denoted herein as ΔR_{ex} . Although ΔR_{ex} (-3.5 ppm) showed a vague signal drop

in the ischemic lesion (Figure 4G), the ischemia-induced signal drop in ΔR_{ex} ($+3.5$ ppm) is much more prominent (Figure 4H).

We further applied the MRAPT analysis to the AREX image $\left(R_1 \cdot \left(\frac{I_0}{I(3.5 \text{ ppm})} - \frac{I_0}{I(-3.5 \text{ ppm})} \right) \right)$. Figure 5A shows the

FIGURE 4 Multiparametric images of pH-sensitive MRI. A, Mean MTR (MMTR) map. B, Calculated $R_{1\rho}$ map. C, The R_1 -scaled inversely normalized Z-spectral map at -3.5 ppm. D, The R_1 -scaled inversely normalized Z-spectral map at $+3.5$ ppm. E, The R_{ex} map at -3.5 ppm. F, The R_{ex} map at $+3.5$ ppm. G, The MT and relaxation-normalized APT (MRAPT) analysis of the R_{ex} map at -3.5 ppm. H, The MRAPT analysis of the R_{ex} map at $+3.5$ ppm

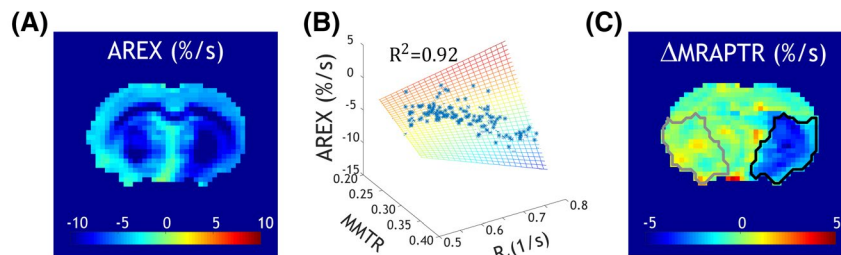
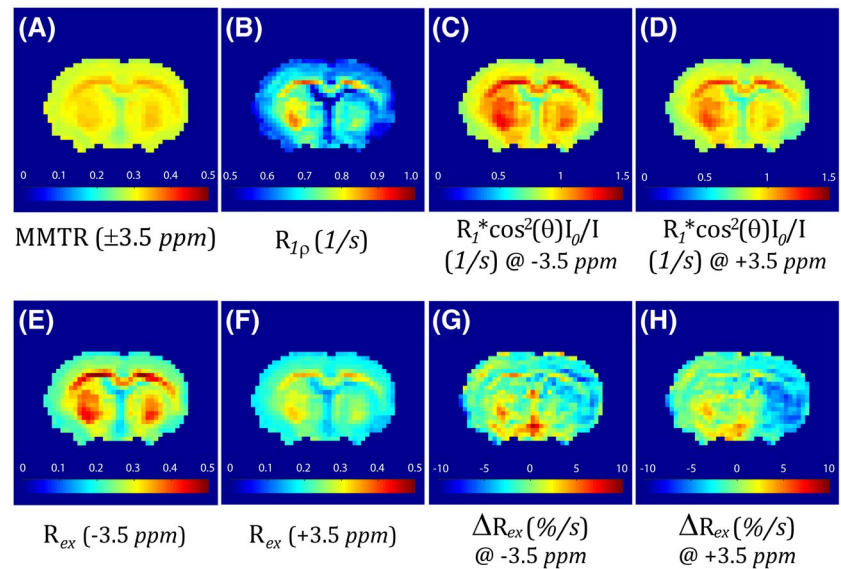


FIGURE 5 Development of pH-specific MRI. A, The apparent exchange-dependent relaxation (AREX) map. B, Regression between AREX and MMTR and R_1 from the contralateral normal brain, per pixel. C, The MRAPT analysis corrects the non-pH baseline variation, yielding a pH-specific MRI map

AREX image, which displays not only ipsilateral hypointensity in the ischemic lesion but also notable heterogeneity in the intact tissue. The AREX, MMTR, and R_1 from the contralateral normal tissue are highly correlated ($R^2 = 0.92$, Figure 5B). Indeed, the MRAPT analysis of the AREX image (Figure 5C) shows reasonably uniform image intensity across the contralateral normal area with a deficit in the ischemic lesion ($0.10 \pm 0.09\%/second$ vs. $-1.99 \pm 0.31\%/second$, $P < .001$). Note that the ipsilateral ischemic lesion (black outline) and contralateral normal region (gray outline) were determined from diffusion MRI (Figure 1) and overlaid on the Δ MRAPTR map. The CNR from MRAPT analysis of the AREX map was 3.03 ± 0.56 , significantly higher than that of the MTR_{asym} image (1.85 ± 0.39 , $P < .001$). Interestingly, the CNRs from the MRAPT analysis of AREX and the $R_{1w} \cdot MTR_{asym}$ (3.01 ± 0.58) images were comparable ($P > .05$).

5 | DISCUSSION

Although both the apparent NOE and APT signals are susceptible to the relaxation-induced symmetric intensity shift,

the calculated R_{ex} spectrum minimizes the confounding T_1 effect. Our work showed that after correcting the relaxation effect, the APT effect is the dominating source of pH-weighted MTR_{asym} contrast in acute stroke. In the original work of Zhou et al, Z-spectrum showed a signal increase only around $+3.5$ ppm (reduced APT effect) with overlapped signals around -3.5 ppm (minimal NOE change), immediately after global ischemia.⁴ Our study is in good agreement with that reported in the global ischemia rat model. Because pH lesion includes both ischemic penumbra and infarction core that are of different pH change, we selected the ischemic diffusion lesion for the ROI analysis. It is also helpful to point out that the derived CEST-MRI effect often depends on the pulse sequence and experimental parameters; therefore, the T_1 contribution needs to be carefully examined.^{45,46}

Although T_1 change has been often reported in experimental stroke imaging,³²⁻³⁶ it has been thought to remain reasonably constant in acute stroke patients. A study from Kauppinen et al may shed some light on this apparent discrepancy between experimental and clinical stroke studies.⁴⁷ Briefly, they showed that the cortical T_1 increased by 4%-7% within a few minutes of global ischemia at 4.7 T and 9.4 T, but

a significantly smaller change (1%-2%) was detected at 1.5 T. Their finding may partially explain why T_1 change was not easily detectable at typical clinical magnetic field strength. Moreover, the lack of interest in T_1 change in the clinic stroke setting could be because diffusion MRI overshadowed the relaxation MRI in the early days of stroke imaging, and subsequent stroke MRI protocols often do not include parametric T_1 mapping.⁴⁸

Although T_1 contribution to conventional Z-spectrum is not straightforward to describe due to the cross terms between multipool CEST and direct RF saturation effects, some qualitative estimation can be performed. Specifically, if we only model the direct RF saturation effect without considering CEST effects, we have $\frac{I(\pm 3.5 \text{ ppm})}{I_0} = \frac{R_1 \cdot \cos^2\theta}{R_1 \cos^2\theta + R_2 \sin^2\theta} = \frac{1}{1 + (T_1/T_2) \cdot \tan^2\theta}$. The T_1 increase in the ischemic tissue results in a slightly more direct RF saturation effect, causing a Z-spectral signal intensity drop of $-0.461\% \pm 0.097\%$ at ± 3.5 ppm, symmetric around the water resonance. The apparent signal intensity change $\left(\Delta \frac{I(\pm 3.5 \text{ ppm})}{I_0}\right)$ on the first-order approximation is a summation of changes from direct RF saturation and CEST effects. After correcting the signal drop due to direct RF saturation, CEST-related Z-spectral signal change at -3.5 ppm $\left(\Delta \frac{I(-3.5 \text{ ppm})}{I_0}\right)$ following acute ischemia became $-0.694\% \pm 0.423\%$, a reduction in its magnitude from that calculated without considering the change in the direct RF saturation effect ($-1.155\% \pm 0.390\%$, Table 1). Moreover, correction of the direct RF saturation-induced intensity drop increased $\Delta \frac{I(+3.5 \text{ ppm})}{I_0}$ from $0.761\% \pm 0.260\%$ (Table 1) to $1.222\% \pm 0.285\%$. Fortunately, a signal change symmetric around the water resonance does not materially affect the magnitude of MTR_{asym} but only the assignment of its origin. This semi-quantitative analysis partially explains why a signal intensity change symmetric around the water resonance reduces the CEST effect at the aliphatic frequency range but strengthens that at the amide proton chemical shift. It is necessary to point out that because the inverse normalization approach simplifies the mathematical modeling of multipool CEST effects, it provides a more quantitative description of pH-weighted MTR_{asym} following acute stroke, as analyzed in our work.

Our study found that the MMTR has a negligible difference between the normal area and ischemic lesion (0.301 ± 0.008 vs. 0.303 ± 0.008), whereas $MTR(-3.5 \text{ ppm})$ was 0.319 ± 0.005 versus 0.330 ± 0.006 , and $MTR(+3.5 \text{ ppm})$ was 0.284 ± 0.01 versus 0.276 ± 0.01 , for the contralateral normal area and ipsilateral ischemic lesion, respectively. This explains why MMTR provides a more reliable correction of the non-pH-dependent baseline image in the MRAPT analysis than $MTR(\pm 3.5 \text{ ppm})$ independently.¹⁶ Our study used a weak RF saturation level of $0.75 \mu\text{T}$ at 4.7 T and concluded that the magnitude of APT signal change is much stronger

than that of the NOE signal. It is worth noting that Heo et al used an RF saturation level of $2 \mu\text{T}$ at 3 T, applied extrapolated semisolid magnetization transfer reference analysis, and concluded that the magnitude of APT change is bigger than that of NOE (-1.45% vs. -1.06%).²¹ However, no significant MTR_{asym} difference between normal and ischemic tissue ($0.78\% \pm 0.33\%$ vs. $0.39\% \pm 0.46\%$) was found. Jin et al calculated the apparent NOE and APT calculation (NOE* and APT*) and showed that unlike APT*, NOE* is not pH-sensitive under a weak RF saturation of $1.25 \mu\text{T}$ at 9.4 T.⁴⁹ In this case, the linear estimation of the reference signal is not susceptible to the T_1 -induced Z-spectral intensity shift. Although these studies used different saturation power levels and field strengths, the results support that APT signal change is more substantial than that of NOE signal following acute stroke, with their relative magnitude being further strengthened when a weak RF saturation pulse is used. It is worth noting that the direct saturation-corrected CEST analysis has been developed to correct the nonlinear direct RF saturation effect, which may augment the APT* and NOE* approach^{49,50} for improved quantification.^{51,52}

The MTR_{asym} calculation, despite its simplicity, provides a reasonable approximation of pH-weighted contrast. Indeed, AREX and $R_{1w} \cdot MTR_{\text{asym}}$ are closely associated with each

other $\left(\text{AREX} = \frac{I_0^2}{I_{\text{ref}} \cdot I_{\text{label}}} \cdot (R_{1w} \cdot MTR_{\text{asym}})\right)$, particularly when

a not too strong B_1 saturation field is used.⁵³ Our study chose an RF saturation power of $0.75 \mu\text{T}$, which maximizes pH-sensitive MTR_{asym} contrast between the ipsilateral ischemic and contralateral normal regions without introducing excessive MT and direct RF saturation effects.⁵⁴ Note that the CNR calculated from background heterogeneity-suppressed MRAPT analysis of AREX and $R_{1w} \cdot MTR_{\text{asym}}$ between the contralateral normal area and ischemic lesion, are comparable.

We calculated Cohen's d to shed light on the size of the contrast, being -3.1 , -7.1 , -3.4 , -10.9 , and -9.3 for perfusion, diffusion, MTR_{asym} , and MRAPT analysis of $R_{1w} \cdot MTR_{\text{asym}}$ and AREX maps, respectively. Cohen's calculation assumes two groups to have similar SDs. Because pH-specific images are rather uniform in the intact tissue due to the MRAPT processing, it is appropriate to use the SD from the ischemic lesion as the best estimate of the pooled SD. This calculation changed Cohen's d to -8.0 and -6.8 for pH-specific MRAPT analysis of $R_{1w} \cdot MTR_{\text{asym}}$ and AREX images, respectively, comparable to that of diffusion MRI. Admittedly, the scan time required for pH-specific MRAPT analysis (APT and T_1 scans) is much longer than that of diffusion MRI (7 minutes 38 seconds vs. 1 minute 44 seconds). As such, pH MRI contrast to noise per unit time (CNR efficiency) is much lower than that of diffusion MRI, as expected. Additional work is needed to shorten pH imaging within 2-3 minutes to facilitate its

adoption in the acute stroke setting. Recently, a fast B_0 field inhomogeneity correction algorithm has been developed that is capable of correcting mild field inhomogeneity without Z-spectrum, which may partially help improve the reproducibility of acute stroke pH imaging in the future.⁵⁵

The pH-specific MRI (Figure 5C) shows graded acidosis, with the most acidification appearing in the striatal area, and a moderate pH drop in the lateral cortex. It is known that for the middle cerebral artery occlusion model, the striatum experiences a worse injury than the cortex, which is more likely to partially reverse following early reperfusion.⁵⁶ Such a mild pH heterogeneity within the diffusion lesion is consistent with reports that the diffusion lesion is not uniform, as measured by lactate MRS⁵⁷ and diffusion kurtosis imaging.^{58,59} Still, the pH heterogeneity within the diffusion lesion is much less than that across the pH lesion, which includes not only the ischemic core but also the metabolic penumbra.¹⁶ This is why we selected the ischemic diffusion lesion for the ROI analysis in our study. In addition to APT and NOE effects at ± 3.5 ppm, our study also captured a definite CEST effect at 2 ppm (Figure 3D), consistent with that of Jin et al.⁶⁰

6 | CONCLUSIONS

Our study elucidated the origin of in vivo MTR_{asym} contrast during the acute stroke and concluded that the APT effect is the dominating source of pH-weighted MTR_{asym} contrast after correcting the relaxation effect. Our finding supports the continued use of MTR_{asym} and amalgamations of it (eg, MRAPT analysis) for pH imaging in the acute stroke setting.

ACKNOWLEDGMENTS

This study was supported in part by a National Institutes of Health grant (R01NS083654 to P.Z.S.). The authors would like to thank Dr. Emiri Mandeville and Dr. Yu Wang for their technical assistance.

ORCID

Phillip Zhe Sun  <https://orcid.org/0000-0003-4872-1192>

REFERENCES

- Tomlinson FH, Anderson RE, Meyer FB. Acidic foci within the ischemic penumbra of the New Zealand white rabbit. *Stroke*. 1993;24:2030-2039; discussion 2040.
- Hossmann KA. Viability thresholds and the penumbra of focal ischemia. *Ann Neurol*. 1994;36:557-565.
- Ward KM, Aletras AH, Balaban RS. A new class of contrast agents for MRI based on proton chemical exchange dependent saturation transfer (CEST). *J Magn Reson*. 2000;143:79-87.
- Zhou J, Payen JF, Wilson DA, Traystman RJ, van Zijl PC. Using the amide proton signals of intracellular proteins and peptides to detect pH effects in MRI. *Nat Med*. 2003;9:1085-1090.
- Jokivarsi KT, Grohn HI, Grohn OH, Kauppinen RA. Proton transfer ratio, lactate, and intracellular pH in acute cerebral ischemia. *Magn Reson Med*. 2007;57:647-653.
- Sun PZ, Benner T, Kumar A, Sorensen AG. Investigation of optimizing and translating pH-sensitive pulsed-chemical exchange saturation transfer (CEST) imaging to a 3T clinical scanner. *Magn Reson Med*. 2008;60:834-841.
- Sun PZ, Sorensen AG. Imaging pH using the chemical exchange saturation transfer (CEST) MRI: Correction of concomitant RF irradiation effects to quantify CEST MRI for chemical exchange rate and pH. *Magn Reson Med*. 2008;60:390-397.
- Sun PZ, Cheung JS, Wang E, Lo EH. Association between pH-weighted endogenous amide proton chemical exchange saturation transfer MRI and tissue lactic acidosis during acute ischemic stroke. *J Cereb Blood Flow Metab*. 2011;31:1743-1750.
- Sun PZ, Wang E, Cheung JS. Imaging acute ischemic tissue acidosis with pH-sensitive endogenous amide proton transfer (APT) MRI—Correction of tissue relaxation and concomitant RF irradiation effects toward mapping quantitative cerebral tissue pH. *NeuroImage*. 2012;60:1-6.
- Schure JR, Shrestha M, Breuer S, et al. The pH sensitivity of APT-CEST using phosphorus spectroscopy as a reference method. *NMR Biomed*. 2019;32:e4125.
- Sun PZ, Zhou J, Sun W, Huang J, van Zijl PC. Detection of the ischemic penumbra using pH-weighted MRI. *J Cereb Blood Flow Metab*. 2007;27:1129-1136.
- Kidwell CS, Alger JR, Saver JL. Evolving paradigms in neuroimaging of the ischemic penumbra. *Stroke*. 2004;35(Suppl 1):2662-2665.
- Tee YK, Harston GWJ, Blockley N, et al. Comparing different analysis methods for quantifying the MRI amide proton transfer (APT) effect in hyperacute stroke patients. *NMR Biomed*. 2014;27:1019-1029.
- Harston GW, Tee YK, Blockley N, et al. Identifying the ischaemic penumbra using pH-weighted magnetic resonance imaging. *Brain*. 2015;138(Pt 1):36-42.
- Msayib Y, Harston GWJ, Tee YK, et al. Quantitative CEST imaging of amide proton transfer in acute ischaemic stroke. *Neuroimage Clin*. 2019;23:101833.
- Guo Y, Zhou IY, Chan ST, et al. pH-sensitive MRI demarcates graded tissue acidification during acute stroke—pH specificity enhancement with magnetization transfer and relaxation-normalized amide proton transfer (APT) MRI. *NeuroImage*. 2016;141:242-249.
- Wang E, Wu Y, Cheung JS, et al. Mapping tissue pH in an experimental model of acute stroke—Determination of graded regional tissue pH changes with non-invasive quantitative amide proton transfer MRI. *NeuroImage*. 2019;191:610-617.
- Sun PZ. Demonstration of magnetization transfer and relaxation normalized pH-specific pulse-amide proton transfer imaging in an animal model of acute stroke. *Magn Reson Med*. 2020 Feb 20. <https://doi.org/10.1002/mrm.28223>.
- Xu J, Zaiss M, Zu Z, et al. On the origins of chemical exchange saturation transfer (CEST) contrast in tumors at 9.4 T. *NMR Biomed*. 2014;27:406-416.
- Zaiss M, Windschuh J, Paech D, et al. Relaxation-compensated CEST-MRI of the human brain at 7T: Unbiased insight into NOE and amide signal changes in human glioblastoma. *NeuroImage*. 2015;112:180-188.

21. Heo HY, Zhang Y, Burton TM, et al. Improving the detection sensitivity of pH-weighted amide proton transfer MRI in acute stroke patients using extrapolated semisolid magnetization transfer reference signals. *Magn Reson Med.* 2017;78:871-880.
22. Wu Y, Zhou IY, Lu D, et al. pH-sensitive amide proton transfer effect dominates the magnetization transfer asymmetry contrast during acute ischemia—quantification of multipool contribution to in vivo CEST MRI. *Magn Reson Med.* 2018;79:1602-1608.
23. Zhou IY, Lu D, Ji Y, et al. Determination of multipool contributions to endogenous amide proton transfer effects in global ischemia with high spectral resolution in vivo chemical exchange saturation transfer MRI. *Magn Reson Med.* 2019;81:645-652.
24. Watanabe T, Frahm J, Michaelis T. Amide proton signals as pH indicator for in vivo MRS and MRI of the brain—Responses to hypercapnia and hypothermia. *NeuroImage.* 2016;133:390-398.
25. Li H, Zu Z, Zaiss M, et al. Imaging of amide proton transfer and nuclear Overhauser enhancement in ischemic stroke with corrections for competing effects. *NMR Biomed.* 2015;28:200-209.
26. Kim J, Wu Y, Guo Y, Zheng H, Sun PZ. A review of optimization and quantification techniques for chemical exchange saturation transfer MRI toward sensitive in vivo imaging. *Contrast Media Mol Imaging.* 2015;10:163-178.
27. Zhou J, Wilson DA, Sun PZ, Klaus JA, Van Zijl PC. Quantitative description of proton exchange processes between water and endogenous and exogenous agents for WEX, CEST, and APT experiments. *Magn Reson Med.* 2004;51:945-952.
28. Wu R, Liu CM, Liu PK, Sun PZ. Improved measurement of labile proton concentration-weighted chemical exchange rate ($k(ws)$) with experimental factor-compensated and T(1)-normalized quantitative chemical exchange saturation transfer (CEST) MRI. *Contrast Media Mol Imaging.* 2012;7:384-389.
29. Zaiss M, Bachert P. Chemical exchange saturation transfer (CEST) and MR Z-spectroscopy in vivo: A review of theoretical approaches and methods. *Phys Med Biol.* 2013;58:R221-R269.
30. Zaiss M, Xu J, Goerke S, et al. Inverse Z-spectrum analysis for spillover-, MT-, and T1-corrected steady-state pulsed CEST-MRI—Application to pH-weighted MRI of acute stroke. *NMR Biomed.* 2014;27:240-252.
31. Zu Z. Towards the complex dependence of MTR_{asym} on T1w in amide proton transfer (APT) imaging. *NMR Biomed.* 2018;31:e3934.
32. Ewing JR, Jiang Q, Boska M, et al. T₁ and magnetization transfer at 7 Tesla in acute ischemic infarct in the rat. *Magn Reson Med.* 1999;41:696-705.
33. Zhang X-Y, Wang F, Afzal A, et al. A new NOE-mediated MT signal at around -1.6 ppm for detecting ischemic stroke in rat brain. *Magn Reson Imaging.* 2016;34:1100-1106.
34. McGarry BL, Jokivarsi KT, Knight MJ, Grohn OHJ, Kauppinen RA. Magnetic resonance imaging protocol for stroke onset time estimation in permanent. *Cerebral Ischemia J Vis Exp.* 2017;2017.
35. Zhou J, Heo H-Y, Knutsson L, van Zijl PC, Jiang S. APT-weighted MRI: Techniques, current neuro applications, and challenging issues. *J Magn Reson Imaging.* 2019;50:347-364.
36. Kaur J, Tuor UI, Zhao Z, Petersen J, Jin AY, Barber PA. Quantified T1 as an adjunct to apparent diffusion coefficient for early infarct detection: A high-field magnetic resonance study in a rat stroke model. *Int J Stroke.* 2009;4:159-168.
37. Young W, Rappaport ZH, Chalif DJ, Flamm ES. Regional brain sodium, potassium, and water changes in the rat middle cerebral artery occlusion model of ischemia. *Stroke.* 1987;18:751-759.
38. Jin T, Autio J, Obata T, Kim SG. Spin-locking versus chemical exchange saturation transfer MRI for investigating chemical exchange process between water and labile metabolite protons. *Magn Reson Med.* 2011;65:1448-1460.
39. Trott O, Palmer AG 3rd. R1rho relaxation outside of the fast-exchange limit. *J Magn Reson.* 2002;154:157-160.
40. Utting JF, Thomas DL, Gadian DG, Helliard RW, Lythgoe MF, Ordidge RJ. Understanding and optimizing the amplitude modulated control for multiple-slice continuous arterial spin labeling. *Magn Reson Med.* 2005;54:594-604.
41. Mori S, Vanzijl PC. Diffusion weighting by the trace of the diffusion tensor within a single scan. *Magn Reson Med.* 1995;33:41-52.
42. Kim M, Gillen J, Landman BA, Zhou J, van Zijl PC. Water saturation shift referencing (WASSR) for chemical exchange saturation transfer (CEST) experiments. *Magn Reson Med.* 2009;61:1441-1450.
43. Sun PZ, Cheung JS, Wang E, Benner T, Sorensen AG. Fast multislice pH-weighted chemical exchange saturation transfer (CEST) MRI with unevenly segmented RF irradiation. *Magn Reson Med.* 2011;65:588-594.
44. Lu D, Jiang Y, Ji Y, et al. Evaluation of diffusion kurtosis imaging of stroke lesion with hemodynamic and metabolic MRI in a rodent model of acute stroke. *AJR Am J Roentgenol.* 2018;210:720-727.
45. Zhao X, Wen Z, Huang F, et al. Saturation power dependence of amide proton transfer image contrasts in human brain tumors and strokes at 3 T. *Magn Reson Med.* 2011;66:1033-1041.
46. Sun PZ, Lu J, Wu Y, Xiao G, Wu R. Evaluation of the dependence of CEST-EPI measurement on repetition time, RF irradiation duty cycle and imaging flip angle for enhanced pH sensitivity. *Phys Med Biol.* 2013;58:N229-N240.
47. Kettunen MI, Gröhn OHJ, Lukkarinen JA, Vainio P, Silvennoinen MJ, Kauppinen RA. Interrelations of T1 and diffusion of water in acute cerebral ischemia of the rat. *Magn Reson Med.* 2000;44:833-839.
48. Nael K, Khan R, Choudhary G, et al. Six-minute magnetic resonance imaging protocol for evaluation of acute ischemic stroke. *Stroke.* 2014;45:1985-1991.
49. Jin T, Wang P, Zong X, Kim SG. MR imaging of the amide-proton transfer effect and the pH-insensitive nuclear Overhauser effect at 9.4 T. *Magn Reson Med.* 2013;69:760-770.
50. Sun PZ, Benner T, Copen WA, Sorensen AG. Early experience of translating pH-weighted MRI to image human subjects at 3 Tesla. *Stroke.* 2010;41(10 Suppl):S147-S151.
51. Zhou Y, Wang E, Cheung JS, et al. Direct saturation-corrected chemical exchange saturation transfer MRI of glioma: Simplified decoupling of amide proton transfer and nuclear Overhauser effect contrasts. *Magn Reson Med.* 2017;78:2307-2314.
52. Wu Y, Chen Y, Zhao Y, et al. Direct radiofrequency saturation corrected amide proton transfer tumor MRI at 3T. *Magn Reson Med.* 2019;81:2710-2719.
53. Jiang W, Zhou IY, Wen L, Zhou X, Sun PZ. A theoretical analysis of chemical exchange saturation transfer echo planar imaging (CEST-EPI) steady state solution and the CEST sensitivity efficiency-based optimization approach. *Contrast Media Mol Imaging.* 2016;11:415-423.
54. Sun PZ, Zhou J, Huang J, van Zijl P. Simplified quantitative description of amide proton transfer (APT) imaging during acute ischemia. *Magn Reson Med.* 2007;57:405-410.
55. Sun PZ. Fast correction of B0 field inhomogeneity for pH-specific magnetization transfer and relaxation normalized amide proton

- transfer imaging of acute ischemic stroke without Z-spectrum. *Magn Reson Med.* 2020;83:1688-1697.
56. Cheung JS, Wang E, Lo EH, Sun PZ. Stratification of heterogeneous diffusion MRI ischemic lesion with kurtosis imaging: Evaluation of mean diffusion and kurtosis MRI mismatch in an animal model of transient focal ischemia. *Stroke.* 2012;43:2252-2254.
 57. Nicoli F, Lefur Y, Denis B, Ranjeva JP, Confort-Gouny S, Cozzone PJ. Metabolic counterpart of decreased apparent diffusion coefficient during hyperacute ischemic stroke: A brain proton magnetic resonance spectroscopic imaging study. *Stroke.* 2003;34:e82-87.
 58. Yin J, Sun H, Wang Z, Ni H, Shen W, Sun PZ. Diffusion kurtosis imaging of acute infarction: Comparison with routine diffusion and follow-up MR imaging. *Radiology.* 2018;287:651-657.
 59. Wang E, Wu Y, Cheung JS, et al. pH imaging reveals worsened tissue acidification in diffusion kurtosis lesion than the kurtosis/diffusion lesion mismatch in an animal model of acute stroke. *J Cereb Blood Flow Metab.* 2017;37:3325-3333.
 60. Jin T, Wang P, Hitchens TK, Kim SG. Enhancing sensitivity of pH-weighted MRI with combination of amide and guanidyl CEST. *NeuroImage.* 2017;157:341-350.

SUPPORTING INFORMATION

Additional Supporting Information may be found online in the Supporting Information section.

FIGURE S1 The T_1 , T_2 , ADC, and pH-weighted magnetization transfer ratio asymmetry (MTR_{asym}) images from a representative acute stroke rat (number 1)

FIGURE S2 The T_1 , T_2 , ADC, and pH-weighted MTR_{asym} images from a representative acute stroke rat (number 2)

FIGURE S3 The T_1 , T_2 , ADC, and pH-weighted MTR_{asym} images from a representative acute stroke rat (number 3)

FIGURE S4 The T_1 , T_2 , ADC, and pH-weighted MTR_{asym} images from a representative acute stroke rat (number 4)

FIGURE S5 The T_1 , T_2 , ADC, and pH-weighted MTR_{asym} images from a representative acute stroke rat (number 5)

FIGURE S6 The T_1 , T_2 , ADC, and pH-weighted MTR_{asym} images from a representative acute stroke rat (number 6)

FIGURE S7 The T_1 , T_2 , ADC, and pH-weighted MTR_{asym} images from a representative acute stroke rat (number 7)

FIGURE S8 The T_1 , T_2 , ADC, and pH-weighted MTR_{asym} images from a representative acute stroke rat (number 8)

FIGURE S9 The T_1 , T_2 , ADC, and pH-weighted MTR_{asym} images from a representative acute stroke rat (number 9)

FIGURE S10 The T_1 , T_2 , ADC, and pH-weighted MTR_{asym} images from a representative acute stroke rat (number 10)

FIGURE S11 Characterization of ischemia-induced CEST Z-spectral signal change from all acute stroke rats. A, The CEST Z-spectra obtained from the contralateral normal area (red) and ipsilateral ischemic region (blue). B, Z-spectral signal change between the contralateral normal area and the ipsilateral ischemic region. C, The MTR_{asym} spectra from the contralateral normal area (red) and ipsilateral ischemic region (blue). D, The MTR_{asym} spectral difference between the contralateral normal area and ipsilateral ischemic lesion. Mean and SDs were plotted

FIGURE S12 Characterization of ischemia-induced inverse CEST Z-spectral signal change from all acute stroke rats. A, The R_1 -scaled inverse CEST Z-spectral changes between the contralateral normal area (red) and ipsilateral ischemic region (blue). B, Intrinsic $R_{1\rho}$ spectral changes between the contralateral normal area and the ipsilateral ischemic region. C, The R_{ex} spectral changes between the contralateral normal area and the ipsilateral ischemic region. D, The R_{ex} spectral difference between the contralateral normal area and ipsilateral ischemic lesion. Mean and SDs were plotted

How to cite this article: Wu L, Jiang L, Sun PZ.

Investigating the origin of pH-sensitive magnetization transfer ratio asymmetry MRI contrast during the acute stroke: Correction of T_1 change reveals the dominant amide proton transfer MRI signal.

Magn Reson Med. 2020;84:2702–2712.

<https://doi.org/10.1002/mrm.28313>